ELSEVIER

International Journal of Heat and Fluid Flow 22 (2001) 402–408

International Journal of HEAT AND FLUID FLOW

www.elsevier.com/locate/ijhff

A nonlinear stress–strain model for wall-bounded turbulent flows ☆

Jens Knoell *, Dale B. Taulbee

Department of Mechanical and Aerospace Engineering, 323 Jarvis Hall, State University of New York at Buffalo, Buffalo, NY 14260, USA

Received 29 November 1999; accepted 19 November 2000

Abstract

A nonlinear stress–strain model, derived from the modeled Reynolds stress transport equation, is modified to account for the near wall effects in wall-bounded turbulent flows. Since it is known that wall reflection of the turbulent pressure field modifies the pressure–strain correlation, the approach taken is to introduce a correction to the coefficients in the closure for the pressure–strain correlation purely based on ideas for full Reynolds stress closures. The stress–strain relation is implemented in the context of the k–ϵ model with a variable C_μ. Results are presented for plane channel flow and both zero and adverse pressure gradient boundary layers. Favorable results for the anisotropies in the Reynolds stresses are obtained by the new model as validated by comparisons against direct numerical simulation (DNS) and experimental data.

Keywords: Turbulence modeling; Stress relation; Wall-bounded flows

1. Introduction

The standard algebraic Reynolds stress model formulation (ARSM) was first developed by Rodi (1972) from the modeled Reynolds stress transport equation, which can be written in terms of the anisotropic stress tensor $a_{ij} = \overline{u_i u_j}/k - 2\delta_{ij}/3$ as

$$k\frac{\mathrm{D}a_{ij}}{\mathrm{D}t} = \frac{\partial T_{ijk}}{\partial x_k} - \frac{\overline{u_i u_j}}{k}\frac{\partial T_l}{\partial x_l} - \frac{\overline{u_i u_j}}{k}(P-\epsilon) + P_{ij} + \Phi_{ij} - \epsilon_{ij}, \tag{1}$$

where $T_{ijk} = -\overline{u_i u_j u_k} - \overline{pu_j}\delta_{ik}/\rho - \overline{pu_i}\delta_{jk}/\rho + \nu\partial\overline{u_i u_j}/\partial x_k$ is the transport, $T_j = T_{ij}/2$, $P_{ij} = -\overline{u_i u_k}\partial U_j/\partial x_k - \overline{u_j u_k}\partial U_i/\partial x_k$ is the production, $P = P_{ii}/2$, Φ_{ij} is the pressure–strain, and ϵ_{ij} is the dissipation tensor. Using energy spectrum measurements it can be argued that the dissipation of turbulent energy occurs predominantly in the small scale range and therefore can be assumed to be isotropic far away from the wall so that $\epsilon_{ij} = 2\epsilon\delta_{ij}/3$. On the other hand all anisotropies in the dissipation occurring in the vicinity of walls can be grouped together with the pressure–strain correlation and approximated by adjusting those coefficients. The pressure–strain Φ_{ij} is modeled in the most general linear way, satisfying only the incompressible continuity equation and symmetry conditions, as

$$\Phi_{ij} = C_0 kS_{ij} - C_1\epsilon a_{ij} + (1-C_3)k\left(a_{il}S_{lj} + a_{jl}S_{li} - \frac{2}{3}a_{lm}S_{ml}\delta_{ij}\right) - (1-C_4)k\left(a_{il}\Omega_{lj} + a_{jl}\Omega_{li}\right), \tag{2}$$

where $\Omega_{ij} = (\partial U_i/\partial x_j - \partial U_j/\partial x_i)/2$ stands for the mean flow vorticity tensor and $S_{ij} = (\partial U_i/\partial x_j + \partial U_j/\partial x_i)/2$ for the mean flow strain rate tensor.

As Taulbee (1992) pointed out the differential equation for a_{ij} can be simplified by assuming a near asymptotic state $\mathrm{D}a_{ij}/\mathrm{D}t \approx 0$ and a small difference in the two transport terms $\partial T_{ijk}/\partial x_k \approx (\overline{u_i u_j}/k)\partial T_k/\partial x_k$. These assumptions are equivalent to Rodi's assumptions and lead to an implicit algebraic equation for a_{ij}

$$\left(C_1 - 1 + \frac{P}{\epsilon}\right)\frac{a_{ij}}{\tau} = -C_3\left(a_{il}S_{lj} + a_{jl}S_{li} - \frac{2}{3}a_{lm}S_{ml}\delta_{ij}\right) + C_4(a_{il}\Omega_{lj} + a_{jl}\Omega_{li}) + \left(C_0 - \frac{4}{3}\right)S_{ij}. \tag{3}$$

In computing a flow field the above equation can in general be solved numerically, however, it is difficult to maintain a stable solution. Therefore, an explicit solution for a_{ij} is desired. Pope (1975) suggested a general solution procedure for this type of formulation and solved the two-dimensional case. Taulbee (1992) was able to extend the solution procedure to the three-dimensional case, solving Eq. (3) for a_{ij}. The exact solution, based on the Cayley–Hamilton theorem, is given as a finite nonlinear tensor polynomial in terms of S_{ij}, Ω_{ij}, and a turbulent time scale $\tau = k/\epsilon$ yielding an explicit nonlinear stress–strain relation for two-dimensional flows,

$$a_{ij} = -2C_\mu\left\{(\tau S_{ij} - C_3 g\tau^2\sigma^2\left(\delta_{ij}^{(2)} - \frac{2}{3}\delta_{ij}^{(3)}\right) + C_4 g\tau^2(S_{il}\Omega_{lj} + S_{jl}\Omega_{li})\right\}, \tag{4}$$

☆ An earlier version of this paper was published in: Engineering Turbulence Modelling and Experiments – 4, eds. W. Rodi and D. Laurence, Elsevier Oxford, 1999, pp. 103–112.

* Corresponding author. Tel.: +49-177-4877158.

E-mail address: jensknoell@mckinsey.com (J. Knoell).

0142-727X/01/$ - see front matter
PII: S0142-727X(00)00085-0

Notation

a_{ij}	anisotropic stress tensor, $a_{ij} = \overline{u_i u_j}/k - 2\delta_{ij}/3$
C_0, C_1, C_3, C_4	pressure–strain coefficients
C_f	skin friction coefficient
$C_{\epsilon 1}$, $C_{\epsilon 2}$, $C_{\epsilon 3}$, $C_{\epsilon 4}$	dissipation equation coefficients
C_μ	turbulent viscosity constant
f_2	Reynolds number dependent function for dissipation equation
f_w	wall function
k	turbulent kinetic energy, $k = \overline{u_i u_i}/2$
P	production rate of k, $P = P_{ii}/2$
P_{ij}	Reynolds stress production, $P_{ij} = -\overline{u_i u_k}\partial U_j/\partial x_k - \overline{u_j u_k}\partial U_i/\partial x_k$
P_ϵ	production rate of dissipation
r	non-dimensional time scale, $r = \tau\sigma$
Re_t	turbulent Reynolds number
Re_θ	Reynolds number based on momentum thickness
Re_τ	Reynolds number based on friction velocity
S_{ij}	mean flow strain rate tensor, $S_{ij} = (\partial U_i/\partial x_j + \partial U_j/\partial x_i)/2$
T_{ijk}	Reynolds stress transport tensor
U_e	freestream velocity
U_i, u_i	mean and fluctuating velocity components
U_τ	friction velocity
$\overline{u_i u_j}$	Reynolds stress tensor
x_i	Cartesian coordinates
y	coordinate normal to the wall
Greeks	
δ	boundary layer thickness
δ_{ij}	Kronecker delta
ϵ	dissipation rate of k, $\epsilon = \epsilon_{ii}/2$
ϵ_{ij}	dissipation tensor
ν	molecular viscosity
ν_t	turbulent viscosity, $\nu_t = C_\mu k^2/\epsilon$
ρ	density
σ	mean flow strain rate invariant, $\sigma^2 = S_{kl}S_{lk}$
τ	turbulent time scale, $\tau = k/\epsilon$
Φ_{ij}	pressure–strain correlation tensor
Ω_{ij}	mean flow rotation rate tensor, $\Omega_{ij} = (\partial U_i/\partial x_j - \partial U_j/\partial x_i)/2$
Superscripts	
$+$	quantity normalized by U_τ and ν

where $\sigma^2 = S_{kl}S_{lk}$, $\omega^2 = \Omega_{kl}\Omega_{lk}$, $g = (C_1 - 1 + P/\epsilon)^{-1}$, $\delta_{ij}^{(2)} = 0$ for $i \neq j$ or $i = j = 3$ and 1 for $i = j = 1$ or 2, $\delta_{ij}^{(3)} = 0$ for $i \neq j$ and 1 for $i = j$, and

$$C_\mu = \frac{(1/2)(4/3 - C_0)g}{1 - (2/3)C_3^2 g^2\tau^2\sigma^2 - 2C_4^2 g^2\tau^2\omega^2}.$$

The ratio P/ϵ is still retained implicitly in the equation so that the formulation turns out to be quasi-explicit since P is a function of $\overline{u_i u_j}$ and therefore also of a_{ij}. In contrast to the quasi-explicit expression in Eq. (4) Girimaji (1996) derived a fully explicit, algebraic expression for the Reynolds stresses with a cubic equation for P/ϵ, which, however, is rather cumbersome to solve for a complex flow field.

2. Calibration of the basic pressure–strain constants

Since the choice of the four coefficients appearing in Eq. (2) is crucial for the performance of the ARSM, care has to be taken in their calibration. Besides the continuity equation and symmetry conditions Rotta (1951) gives an additional constraint, which is commonly referred to as normalization condition. It is a consequence of applying Green's theorem to the rapid part of the pressure–strain correlation. Utilizing this condition relates C_3 and C_4 to a single constant C_2 as

$$C_3 = (5 - 9C_2)/11, \quad \text{and} \quad C_4 = (1 + 7C_2)/11. \tag{5}$$

Furthermore, it restricts C_0 to the value of 0.8 independent of the choice of C_2 as discussed by Launder et al. (1975). However, since most flow fields are non-homogeneous a relaxation of the normalization constraint turns out to be necessary to improve the predictive capabilities of second moment closures and therefore, the simplifications in Eq. (5) are not applied. Nevertheless, the constant C_0 is chosen to be 0.8 in the present formulation to reproduce the correct response of isotropic turbulence to an imposed mean strain rate according to Crow (1968). The remaining three coefficients are calibrated against the DNS data for the equilibrium region of a fully developed channel flow for two different Reynolds numbers by Kim et al. (1987) and against experimental and numerical homogeneous shear flow data by Tavoularis and Corrsin (1981), Tavoularis and Karnik (1989), Harris et al. (1977), Rose (1966) and Rogers et al. (1986). From the experimental data for the Reynolds stresses and the strain field 3 independent pressure–strains (Φ_{11}, Φ_{22}, and Φ_{12}) can be determined in the two-dimensional case by fitting the downstream evolution in the experiment with the pressure–strain model as given in Eq. (2). The unknown coefficients C_i are determined by a least-square optimization for each experiment and finally averaged for the different experimental cases. Thus, this procedure is performed on a Reynolds stress closure level and not influenced by the approximations leading to the ARSM. The resulting values are $C_1 = 1.47$, $C_3 = 0.19$, and $C_4 = 0.41$.

3. Realizability of the wall independent ARSM

To ensure physical results for the Reynolds stresses in complex strain fields the ARSM has to satisfy the constraints of realizability, which require non-negative normal stresses and the observance of the Schwarz inequality for the off-diagonal components of $\overline{u_i u_j}$. These conditions have been discussed by Schumann (1977) in detail. Fig. 1 shows the development of the non-dimensional normal stresses $\overline{u_\alpha u_\alpha}/k$ (no summation over α) and of the quantity $\overline{uv}^2/(\overline{u^2}\,\overline{v^2})$ with respect to a non-dimensional time scale $r = \tau\sigma$ for the ARSM in the homogeneous shear flow case. The results for the ARSM obtained from Eq. (4) are compared to experimental data for various homogeneous shear flows. It can be seen that the agreement with the experiments is very good. Furthermore, since the normal stresses asymptotically approach a value larger than 0 and $\overline{uv}^2/(\overline{u^2}\,\overline{v^2})$ tends to a value of 0.3 the realizability constraints are satisfied for the ARSM with the calibrated set of pressure–strain coefficients.

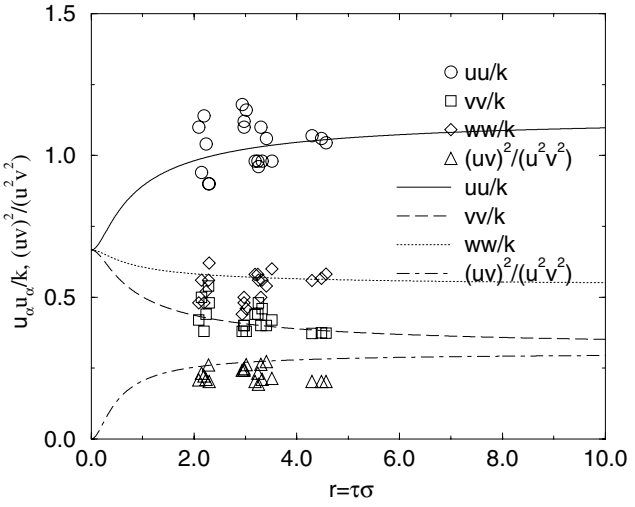

Fig. 1. Realizability for homogeneous shear flows: Symbols, experimental data by Tavoularis and Corrsin (1981), Tavoularis and Karnik (1989), and Harris et al. (1977); lines, computations for the ARSM.

4. Modifications of the ARSM for wall-bounded flows

In the vicinity of the wall the pressure–strain components are strongly influenced by the wall reflection of the turbulent pressure field and by viscous effects. These effects combined with non-homogeneities, which are not described by the wall-independent pressure–strain correlation, need to be modeled in wall-bounded turbulent flows. Thus, following an approach taken by Launder and Shima (1989) for second moment closures the total pressure–strain correlation can be divided into two parts, namely a basic wall independent part Φ_{ij}^{o} and a wall dependent part Φ_{ij}^{w}, which represents the effects created in the presence of the wall

$$\Phi_{ij} = \Phi_{ij}^{\mathrm{o}} + \Phi_{ij}^{\mathrm{w}}. \tag{6}$$

Even though the general linear pressure–strain correlation in Eq. (2) is not able to account for the wall effects, second moment closures and therefore the ARSM are also used for predicting nonhomogeneous flow fields, such as a boundary layer and the near wall region in a channel flow. As a consequence additional degrees of freedom have to be created by Φ_{ij}^{w}. Furthermore, the anisotropies in ϵ are grouped together with the wall dependent pressure–strain part Φ_{ij}^{w}. Since the exact processes of the wall reflection of the turbulent pressure field cannot be resolved by the considered turbulence model, empirical functions have to be introduced in the formulation of Φ_{ij}^{w}. Assuming the same functional form for Φ_{ij}^{o} and Φ_{ij}^{w} yields for the coefficients

$$C_i = C_{i\mathrm{o}} + C_{i\mathrm{w}} f_{\mathrm{w}}, \tag{7}$$

where $i = 1, 2, 3, 4$, so that the empirical dependence on the wall is grouped inside a wall function f_{w}. Therefore, the pressure–strain coefficients consist of a wall independent part $C_{i\mathrm{o}}$, which has already been calibrated against homogeneous shear flows and the equilibrium region of channel flows, and a wall dependent part $C_{i\mathrm{w}} f_{\mathrm{w}}$. Physical arguments support the idea that the effects of the wall have to disappear with an increasing distance from the wall and have to be stronger adjacent to the wall. Therefore, the use of the standard wall function $f_{\mathrm{w}} = \exp(-y^+/B^+)$ in terms of the wall coordinate $y^+ = U_\tau y/\nu$, with B^+ denoting an adjustable constant, is an obvious choice and frequently used in near wall models. However, these models cannot be applied to flows in complex geometries, where a unique wall distance does not exist. As a quantity that is independent of the wall distance the turbulent time scale $\tau^+ = k^+/\epsilon^+$, with $k^+ = k/U_\tau^2$, and $\epsilon^+ = \epsilon\nu/U_\tau^4$, is implemented in the wall function $f_{\mathrm{w}} = \exp(-\tau^+/A^+)$, with $A^+ = 60$, leading to a more general model applicable to all geometries. To simplify the formulation the same wall function f_{w} is used for all wall coefficients $C_{i\mathrm{w}}$. This methodology allows the derivation of a nonlinear stress–strain relation of the form given in Eq. (4) but including near-wall effects. In contrast to many previous model suggestions all new model constants are systematically introduced. As a result the new model is fully consistent with differential Reynolds stress models. The advantage is now that different modeling ideas stemming from full Reynolds stress closures allow the assumption of compatibility also on the two-equation model level.

5. Calibration of the wall dependent coefficients

This section is based on certain compatibility conditions that need to be satisfied at the wall. Eq. (7) shows that four additional coefficients appear in the wall dependent pressure–strain part. From Taylor series expansions of the fluctuation velocities at the wall (e.g., Chien, 1982) and continuity constraints it can be deduced that $u \sim y$, $v \sim y^2$ and therefore, $\overline{uv} \sim y^3$. This argument further yields $k \sim y^2$ and $\epsilon \sim y^0$. The mean velocity goes as $U \sim y$, thus the gradient $(\partial U/\partial y) \sim 1$. The Boussinesque approximation leads to $\nu_{\mathrm{t}} \sim y^3$, so that finally $C_\mu \sim 1/y$, since $C_\mu = \nu_{\mathrm{t}}\epsilon/k^2$. The asymptotic behavior *very near the wall* can only be represented if the function g in the formulation for C_μ goes as $1/y$ in the vicinity of the wall. Since the production P disappears and ϵ reaches a finite value, the condition

$$\lim_{y\to 0} C_1 = 1 \to C_{1\mathrm{w}} = 1 - C_{1\mathrm{o}}$$

must be satisfied for consistency of the model at the wall, so that $C_{1\mathrm{w}}$ is determined. $C_{0\mathrm{w}}$, $C_{3\mathrm{w}}$ and $C_{4\mathrm{w}}$ remain to be calibrated against a wall dependent flow field. The set $C_{0\mathrm{w}} = 0.211$, $C_{3\mathrm{w}} = 0.71$ and $C_{4\mathrm{w}} = 0.275$ is the result from the calibration of the coefficients with the fully developed channel flow and obtained by optimizing the mean velocity and the Reynolds shear stress and simultaneous adjusting the level of anisotropies of the normal stresses in the wall region. The same set of constants is kept for the zero pressure gradient boundary layer (ZPG) and the adverse pressure gradient boundary layer (APG) case. The wall dependent ARSM formulation also has to satisfy the realizability constraints. In a general two-dimensional incompressible flow the velocity field depends on three independent strain components, which can be grouped together to two non-dimensional quantities describing the relative effects of the different strains. Additionally a_{ij} in Eq. (4) depends on the non-dimensional time scale r and the value of f_{w}, which influences the pressure–strain coefficients. Therefore, four independent quantities determine the Reynolds stress tensor in the ARSM. The numerical approach taken is to vary the four quantities and search for the extrema in the four-dimensional space. In this way it was ensured that all energy components are non-negative and that the Schwarz inequality is satisfied for the given set of coefficients.

6. Corresponding k–ϵ model

The kinetic energy equation is modeled in the traditional way as

$$\frac{Dk}{Dt} = \frac{\partial}{\partial x_j}\left[\left(\frac{\nu_t}{\sigma_k} + \nu\right)\frac{\partial k}{\partial x_j}\right] + P - \epsilon, \tag{8}$$

with $\nu_t = C_\mu k^2/\epsilon$ and $\sigma_k = 1.0$. The high Reynolds number transport equation for the dissipation ϵ is modified in three ways to include near wall effects. First, the coefficient of the decay term is made Reynolds number dependent with the function f_2 following Hanjalic and Launder (1976). Secondly, the same authors suggested to retain a secondary source term appearing in the exact transport equation and to model it as

$$2\nu\overline{u_l\frac{\partial u_i}{\partial x_j}}\frac{\partial^2 U_i}{\partial x_l \partial x_j} = C_{\epsilon 3}\nu\nu_t\left(\frac{\partial^2 U_i}{\partial x_j \partial x_l}\right)^2.$$

Finally, the time scale is changed according to Durbin (1993)

$$\tau_\epsilon = \mathrm{MAX}\left[\frac{k}{\epsilon}; C_T\sqrt{\frac{\nu}{\epsilon}}\right],$$

so that τ_ϵ is identical to the standard time scale k/ϵ over most parts of the flow. However, adjacent to the wall, where the flow field is dominated by viscous effects, τ_ϵ switches to the finite viscous time scale. Thus, the dissipation equation reads

$$\frac{D\epsilon}{Dt} = \frac{\partial}{\partial x_j}\left[\left(\nu + \frac{\nu_t}{\sigma_\epsilon}\right)\frac{\partial \epsilon}{\partial x_j}\right] - C_{\epsilon 1}\frac{\overline{u_i u_j}}{\tau_\epsilon}\frac{\partial U_i}{\partial x_j} - C_{\epsilon 2} f_2 \frac{\epsilon}{\tau_\epsilon} + C_{\epsilon 3}\nu\nu_t\left(\frac{\partial^2 U_i}{\partial x_j \partial x_l}\right)^2, \tag{9}$$

where $f_2 = 1 - 2/9\exp[-(Re_t/6)^2]$ and $\sigma_\epsilon = 1.3$, $C_T = 3.0$, $C_{\epsilon 1} = 1.44$, $C_{\epsilon 2} = 1.9$, and $C_{\epsilon 3} = 1.0$. Eq. (9) works well for channel flows and the ZPG boundary layer. However, as discussed in detail by Rodi and Scheuerer (1986) problems arise if a k–ϵ type model is used in an adverse pressure gradient flow. Hanjalic and Launder (1980) recommended the artificial enhancement of the production of dissipation, originating in the irrotational strain part, by a factor $C_{\epsilon 4}$ so that the total production of dissipation reads in the APG case

$$P_\epsilon = -C_{\epsilon 1}\frac{\overline{uv}}{\tau_\epsilon}\frac{\partial U}{\partial y} - C_{\epsilon 4}\frac{1}{\tau_\epsilon}(\overline{uu} - \overline{vv})\frac{\partial U}{\partial x} + C_{\epsilon 3}\nu\nu_t\left(\frac{\partial^2 U}{\partial y^2}\right)^2,$$

with $C_{\epsilon 4} = 3.5$, which works better for the ARSM than the original value of $C_{\epsilon 4} = 4.44$ as suggested by Hanjalic and Launder (1980). The irrotational strain term has no influence on the ZPG boundary layer and the channel flow since $\partial U/\partial x \ll \partial U/\partial y$ in the boundary layer and $\partial U/\partial x = 0$ in the channel flow. Furthermore, the second derivative in the x-direction $\partial^2 U/\partial x^2$ and the mixed derivative $\partial^2 U/\partial x \partial y$ appearing in the last term of Eq. (9) are negligible compared to $\partial^2 U/\partial y^2$ in the boundary layer case and identically zero in the channel flow. As a consequence the choice of $C_{\epsilon 4}$ has no influence on the ZPG boundary layer and the channel flow computations since the irrotational strain term in the production of ϵ can be neglected.

7. Discussion of computed results

Figs. 2–4 show the computed results for a fully developed channel flow at $Re_\tau = 180$ compared to the DNS data by Kim et al. (1987). The mean velocity and shear stress computed by the model are in excellent agreement with the DNS data. For the normal stresses the ARSM is able to reproduce the data well for $y^+ > 50$. However, close to the wall the anisotropies of the Reynolds stress tensor are not fully resolved. In this region the turbulent transport is likely to play a dominant role and therefore, most algebraic Reynolds stress closures fail to accurately predict $\overline{u_\gamma u_\alpha}$. Thus, the variable pressure–strain coefficients in Φ_{ij} are obviously not sufficient to compute the anisotropies close to the wall. Finally, Fig. 5 shows reasonable agreement of the skin friction computation with the experimental data compiled by Dean (1978).

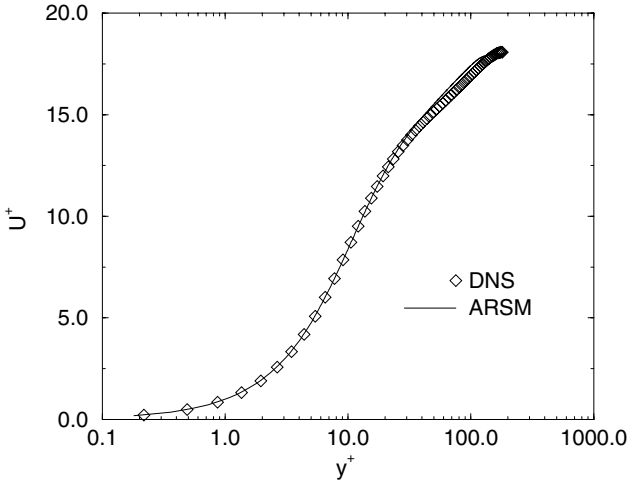

Fig. 2. Mean velocity for a turbulent channel flow at $Re_\tau = 180$ compared to DNS data by Kim et al. (1987).

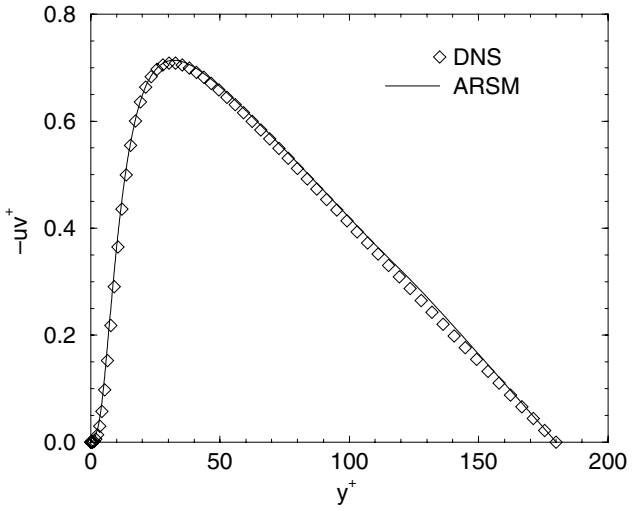

Fig. 3. Reynolds shear stress for a turbulent channel flow at $Re_\tau = 180$ compared to DNS data by Kim et al. (1987).

Figs. 6–11 show the results of the calculations for the two boundary layer cases. Unlike the channel flow both boundary layers represent evolving flows with downstream gradients. First, the ZPG boundary layer at $Re_\theta = 7700$ is computed and compared to experimental results by Klebanoff (1954). As in the channel flow case the mean velocity and the Reynolds shear stress show good agreement with the data while the ARSM is not able to completely reproduce the anisotropies in the normal stresses.

Furthermore, an APG boundary layer case according to the experiment by Andersen et al. (1972) is predicted by the model. This flow can be considered a non-trivial test case of uttermost importance for aerodynamic computations. However, it is striking that APG boundary layers are quite often not the topic of the turbulence model validation. All quantities are normalized with the freestream velocity U_e and the boundary layer thickness δ. In agreement with the discussion by Rodi

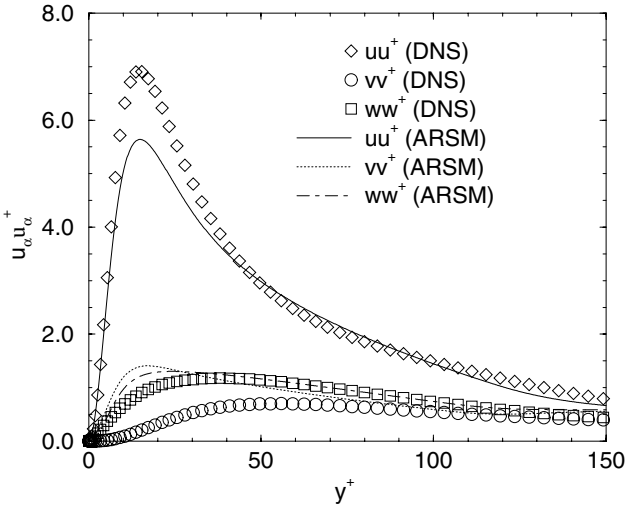

Fig. 4. Reynolds normal stresses for a turbulent channel flow at $Re_\tau = 180$ compared to DNS data by Kim et al. (1987).

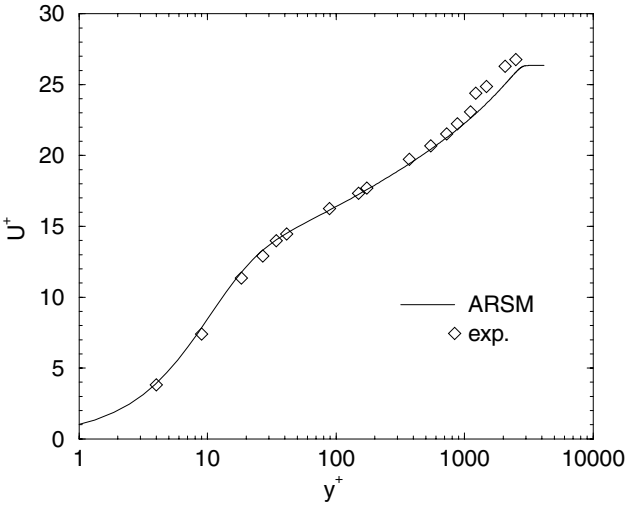

Fig. 6. Mean velocity for a zero pressure gradient boundary layer at $Re_\theta = 7700$ compared to experimental data by Klebanoff (1954).

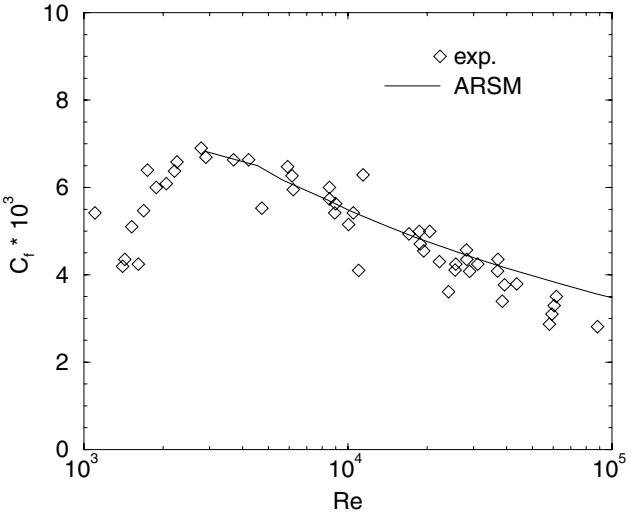

Fig. 5. Skin friction coefficient for a turbulent channel flow compared to experimental data compiled by Dean (1978).

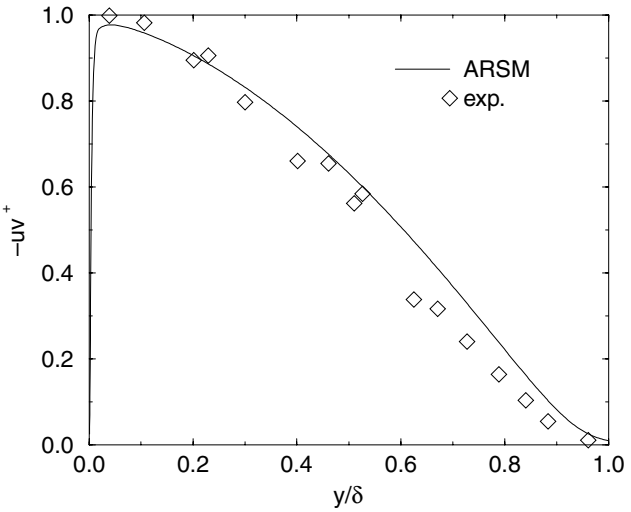

Fig. 7. Reynolds shear stress for a zero pressure gradient boundary layer at $Re_\theta = 7700$ compared to experimental data by Klebanoff (1954).

and Scheuerer (1986) for standard low Reynolds number k–ϵ models the ARSM also suffers from inaccuracies in the APG case. Close to the wall both the mean velocity and the shear stress differ from the measurements while the agreement is very good towards the outside of the boundary layer. The last plot for the Reynolds normal stresses shows again that the modification in the pressure–strain correlation is insufficient to completely capture the anisotropies in the normal stresses for wall-bounded turbulent flows. It seems that the transport effects in Eq. (1) need to be included in some way in the stress–strain relation to improve the quality of the predictions.

8. Summary

The algebraic stress model with the corresponding stress–strain relation, which has been developed from the modeled Reynolds stress transport equation, is modified to account for the near wall effects in wall-bounded turbulent flows. These modifications include the implementation of a general linear pressure–strain correlation with carefully calibrated coefficients leading to a model that is realizable for the general two-dimensional case. Additionally, Reynolds stress modeling ideas for the pressure–strain correlation in the near wall region are also used to reduce the number of ad hoc functions in the closure. Only one empirical function, which is wall distance free and in terms of the turbulent time scale, is used to account for near wall effects in the stress–strain relation. In contrast to systematic expansions of the Reynolds stresses as a function of the mean velocity gradient and scalars describing the turbulent scales the solution to the implicit algebraic stress model leads to a logically consistent stress–strain relation with all coefficients determined by the underlying models for the PS and the dissipation equation. Further improvements focus on a more accurate representation of the modeled dissipation equation considering a modified time scale and a Reynolds number dependent dissipation term. Beside the classical examples of channel flows and ZPG boundary layers the model is also tested for an APG boundary layer, where the normal stresses

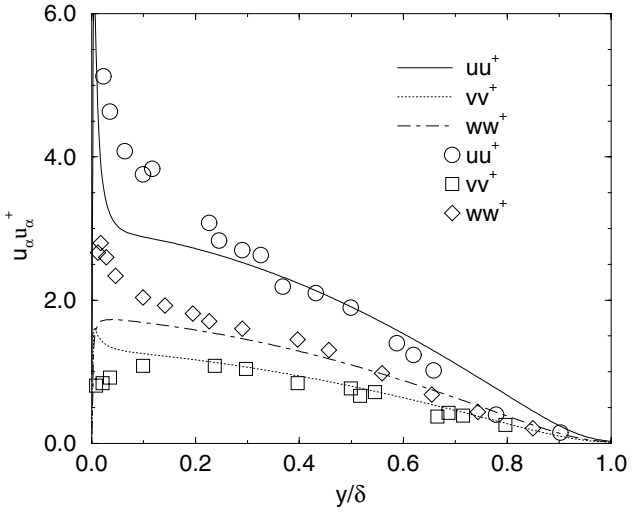

Fig. 8. Reynolds normal stresses for a zero pressure gradient boundary layer at $Re_\theta = 7700$ compared to experimental data by Klebanoff (1954).

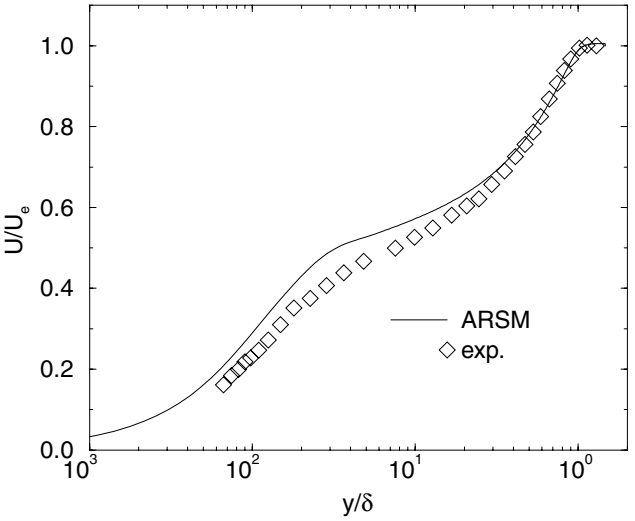

Fig. 9. Mean velocity for an adverse pressure gradient boundary layer at $Re_\theta = 3673$ compared to experimental data by Andersen et al. (1972).

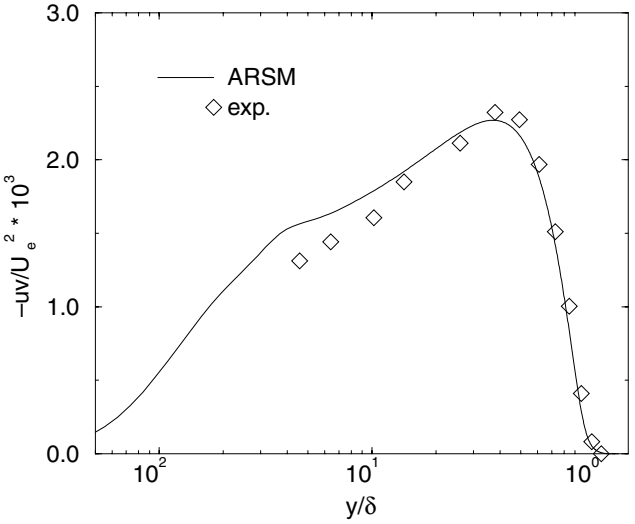

Fig. 10. Reynolds shear stress for an adverse pressure gradient boundary layer at $Re_\theta = 3673$ compared to experimental data by Andersen et al. (1972).

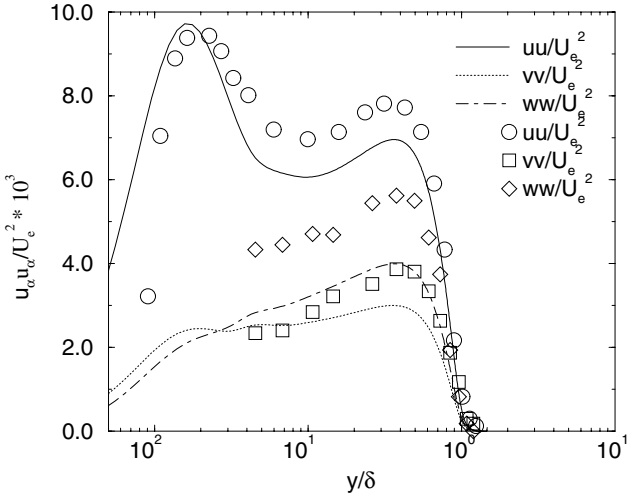

Fig. 11. Reynolds normal stresses for an adverse pressure gradient boundary layer at $Re_\theta = 3673$ compared to experimental data by Andersen et al. (1972).

have a significant effect on the evolution of the mean velocity profile along the plate. For the APG case an enhancement of the irrotational strain contribution to the production of dissipation term is found to be necessary as discussed by Hanjalic and Launder (1980). The main objective of the new model to improve the representation of the anisotropies in the Reynolds stresses compared to standard k–ϵ models is achieved as shown by the comparison to various flows. Unlike full differential Reynolds stress closures, where differential transport equations for $\overline{uu}$, $\overline{vv}$, $\overline{ww}$, $\overline{uv}$, and ϵ have to be solved in the two-dimensional case, the new model only requires the solution of two differential equations for k and ϵ and explicit algebraic stress–strain relations for the Reynolds stresses. The latter algebraic equations are in their complexity identical to nonlinear two-equation models. The only increase in computational effort is due to the iteration over P/ϵ. However, the iteration converges quickly after very few iteration steps.

References

Andersen, P.S., Kays, W.M., Moffat, R.J., 1972. The turbulent boundary layer on a porous plate: an experimental study of the fluid mechanics for adverse free-stream pressure gradients. Stanford Report No. HMT-15.

Chien, K.Y., 1982. Prediction of channel and boundary layer flows with a low-Reynolds-number turbulence model. AIAA Journal 20, 33–38.

Crow, S.C., 1968. Viscoelastic properties of fine-grained incompressible turbulence. Journal of Fluids Mechanics 33, 1–20.

Dean, R.B., 1978. Reynolds number dependence of skin friction and other bulk flow variables in two-dimensional rectangular duct flow. Journal of Fluids Engineering 100, 215–223.

Durbin, P.A., 1993. Application of a near-wall turbulence model to boundary layers and heat transfer. International Journal of Heat and Fluid Flow 14, 316–323.

Girimaji, S.S., 1996. Fully explicit and self-consistent algebraic stress model. Theoretical and Computational Fluid Dynamics 8, 387–402.

Hanjalic, K., Launder, B.E., 1976. Contribution towards a Reynolds-stress closure for low-Reynolds-number turbulence. Journal of Fluid Mechanics 74, 593–610.

Hanjalic, K., Launder, B.E., 1980. Sensitizing the dissipation equation to irrotational strains. Journal of Fluids Engineering 102, 34–40.

Harris, V.G., Graham, A.H., Corrsin, S., 1977. Further experiments in nearly homogeneous turbulent shear flow. Journal of Fluid Mechanics 81, 657–687.

Kim, J., Moin, P., Moser, R., 1987. Turbulence statistics in fully developed channel flow at low Reynolds number. Journal of Fluid Mechanics 177, 133–166.

Klebanoff, P.S., 1954. Characteristics of turbulence in a boundary layer with zero pressure gradient. NACA Technical Notes No. 3178.

Launder, B.E., Reece, J., Rodi, W., 1975. Progress in the development of a Reynolds-stress turbulence closure. Journal of Fluid Mechanics 68, 537–566.

Launder, B.E., Shima, N., 1989. Second-moment closure for the near-wall sublayer: development and application. AIAA Journal 27, 1319–1325.

Pope, S.B., 1975. A more general effective-viscosity hypothesis. Journal of Fluid Mechanics 72, 331–340.

Rodi, W., 1972. The prediction of free turbulent boundary layers by use of a two equation model of turbulence. Ph.D. Thesis, University of London, London, England.

Rodi, W., Scheuerer, G., 1986. Scrutinizing the k–ϵ turbulence model under adverse pressure gradient conditions. Journal of Fluids Engineering 108, 174–179.

Rogers, M.M., Moin, P., Reynolds, W.C., 1986. The structure and modeling of the hydrodynamic and passive scalar fields in homogeneous turbulent shear flow. Stanford Report No. TF-25.

Rose, W.G., 1966. Results of an attempt to generate a homogeneous turbulent shear flow. Journal of Fluid Mechanics 25, 97–120.

Rotta, J., 1951. Statistische Theorie nichthomogener Turbulenz. Zeitschrift für Physik 129, 547–572.

Schumann, U., 1977. Realizability of Reynolds stress turbulence models. Physics of Fluids A 20, 721–725.

Taulbee, D.B., 1992. An improved algebraic Reynolds stress model and corresponding nonlinear stress model. Physics of Fluids A 4, 2555–2561.

Tavoularis, S., Corrsin, S., 1981. Experiments in nearly homogeneous turbulent shear flow with a uniform mean pressure gradient. Part 1. Journal of Fluid Mechanics 104, 311–347.

Tavoularis, S., Karnik, U., 1989. Further experiments on the evolution of turbulent stresses and scales in uniformly sheared turbulence. Journal of Fluid Mechanics 204, 457–478.